FLOW OF A PLANAR SHOCK WAVE AROUND A THERMAL LAYER AT A RIGID WALL

B. I. Zaslavskii, S. Yu. Morozkin,
A. A. Prokof'ev, and V. R. Shlegel'

UDC 533.6.011.72

There are several papers [1-9] on the wave structure of the flow arising when a planar shock wave (SW) interacts with a rigid wall covered by a low-density gas; the sliding mode of motion along the wall has been examined. The fullest exposition is given in [6, 9], where computations were reported on the density and pressure patterns behind the perturbed part of the SW front for the initial parameters $M_1 = 2$, $\rho_Q/\rho_0 = 1/3$ [6]; $M_1 = 32$, $\rho_Q/\rho_0 = 1/3$ [9] (M_1 is the Mach number in the SW and ρ_Q/ρ_0 is the ratio of the densities in the layer and outside it).

The same formulation has also been used in calculations for $M_1 = 1.44$, $M_1 = 1.33$ [4], where the wave patterns as computed were compared with Töpler photographs. In [8], the interaction was examined for wide ranges in M_1 and ρ_Q/ρ_0 by experiment. A somewhat different case was considered in [5, 7, 8], where SW motion along a suddenly heated surface was examined. There was a thin layer of hot gas at the reflecting surface, but a difference from [4, 6, 8, 9] was that the layer was inhomogeneous, as it was unevenly heated, and there was no density step.

We have made measurements on the interaction of a planar SW with a wall layer of low-density gas (wall thermal) for a wide range of angles of incidence, wall-layer densities, and SW intensities. A theoretical analysis is also presented for the wave structure.

1. Consider a planar infinitely-long SW moving with speed N_1 in the half-space $y > -x \tan\alpha$ (Fig. 1a), which is filled by a gas having initial density ρ_0, pressure p_0, temperature T_0, and initial speed of sound c_0. Behind the SW front, the pressure is p_1 and the particle speed q_1. We introduce the dimensionless parameter $\varepsilon_1 = (p_1 - p_0)/np_0$ (n is the adiabatic parameter). Then [10]

$$N_1 = c_0\sqrt{1+\frac{n+1}{2}\varepsilon_1},\quad q_1 = c_0\varepsilon_1\Big/\sqrt{1+\frac{n+1}{2}\varepsilon_1}. \tag{1.1}$$

On the axis $x = 0$ and $y = 0$, the plane $y = -x\tan\alpha$ intersects the rigid wall S (half-plane $y = 0$, $x > 0$). When the shock front arrives at point d ($t = 0$), a thermal arises suddenly above S: a layer Q (dd_1d_2, Fig. 1) of gas having $\rho_Q < \rho_0$, p_0, and $c_Q > c_0$, and with free boundaries dd_1 and d_1d_2. The equations for those surfaces for $t = 0$ are $y = x\cot\alpha$, $y = h$, $x > h\tan\alpha$.

We consider the motion for $t > 0$. When the shock front reaches the interface dd_1, the latter becomes a surface of discontinuity for the two states. The decay of that discontinuity gives rise to a negative-pressure wave in the external gas and an SW precursor [1-3, 5, 6], which runs ahead of the main wave in the layer Q. The parameters of those waves at the start can be determined for various c_Q/c_0 and ε_1 by the p–q diagram method [10], which we use on the basis that the contact discontinuity line is subject to the conditions

$$p_r = p_Q^0,\quad q_r = q_Q^0 \tag{1.2}$$

(p_r, p_Q^0, q_r, q_Q^0 are correspondingly the pressure and the particle velocity for the heavy and light gases adjoining the contact discontinuity line), which gives [8]

$$q_r = \frac{c_0\varepsilon_1}{\sqrt{1+\frac{n+1}{2}\varepsilon_1}} + \frac{2c_0}{n-1}\sqrt{\frac{(1+n\varepsilon_1)\left(1+\frac{n-1}{2}\varepsilon_1\right)}{1+\frac{n+1}{2}\varepsilon_1}\left[1-\left(\frac{1+n\varepsilon_r}{1+n\varepsilon_1}\right)^{(n-1)/2n}\right]} = \frac{nc_Q\varepsilon_r}{n_Q\sqrt{1+\frac{n(n_Q+1)}{2n_Q}\varepsilon_r}}. \tag{1.3}$$

Mendeleevo. Translated from Zhurnal Prikladnoi Mekhaniki i Tekhnicheskoi Fiziki, No. 3, pp. 15-23, May-June, 1990. Original article submitted March 4, 1988.

 0021-8944/90/3103-0354$12.50

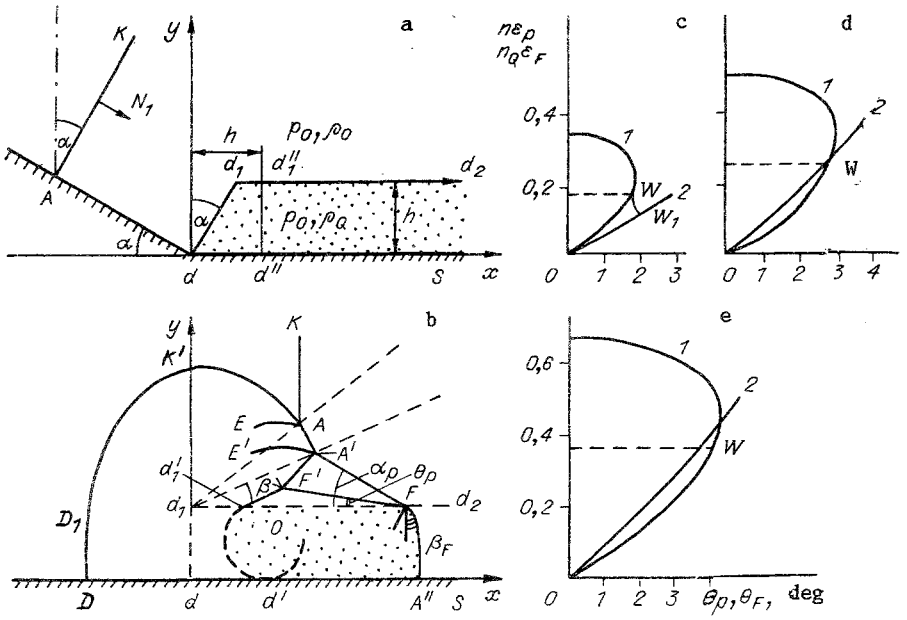

Fig. 1

Here $\varepsilon_r = (p_r - p_0)/np_0$ is the relative pressure in the flow passing through the negative-pressure wave DD_1 and n_Q is the adiabatic parameter for the light gas.

Conditions (1.2) remain correct for small t, and in any case for $0 < t < t_1$, where t_1 is the instant when the acoustic perturbation from point d_1 arrives at S. There is subsequently a complicated three-dimensional motion, whose supposed shock-wave structure is shown in Fig. 1.

We consider the head part for glancing indicence ($\alpha = 0$). The shock wave FA" (Fig. 1b) propagates in the layer with velocity $N_{A"} > N_1$ and creates a perturbed region A'FF' outside the layer ahead of the front AK (the shock fronts A'F and A'F' and the contact surface FF'). A'F and the flow behind it should be conjugate to the flow behind FA". The conjugation conditions at point F, where the two fronts meet, will be as follows if the velocity vectors for the flows arriving at F from the fronts A'F and FA" are collinear and the pressures behind those fronts are equal:

$$n\varepsilon_p = n_Q\varepsilon_F, v_p(N_{A''} - u_F) = v_F(N_{A''} - u_p). \tag{1.4}$$

Here u_p, v_p, u_F, v_F are the particle velocity components, while ε_p and ε_F are the relative pressure differences near F behind the fronts A'F and FA".

The conjugation conditions may differ substantially from Eq. (1.4) because the negative-pressure wave may become centered between those fronts.

Which of the two states occurs can be determined by the shock-polar method with p and θ as coordinates (θ is the angle of rotation for the flow that has passed through the shock front) [10]. The equations for those polars in the above symbols are

$$\operatorname{tg}\theta_p = \frac{\varepsilon_p}{M_p^2 - \varepsilon_p}\sqrt{\frac{M_p^2 - 1 - \frac{n+1}{2}\varepsilon_p}{1 + \frac{n+1}{2}\varepsilon_p}},$$

$$\operatorname{tg}\theta_F = \frac{\varepsilon_F}{M_F^2 - \varepsilon_F}\sqrt{\frac{M_F^2 - 1 - \frac{n_Q+1}{2}\varepsilon_F}{1 + \frac{n_Q+1}{2}\varepsilon_F}}, \quad M_F = M_p c_0/c_Q,$$

in which M_p and M_F are the Mach numbers for the flows ahead of A'F and FA" in the coordinate system linked to F, while θ_p and θ_F are the angles of rotation for the flows at those fronts.

Parts c and d of Fig. 1 show two forms for the SW polars intersecting at F, which have been constructed with $n\varepsilon$ and θ as coordinates: curves 1 are those for the flow in layer Q and curves 2 for the external flow.

In Fig. 1c, the polar curve for the external flow does not intersect the shock polar for the flow in layer Q. The flows behind the corresponding fronts can be linked only via the centered negative-pressure wave, which here corresponds to the WW_1 curve. Point M on the shock polar for the flow in layer Q should correspond to the acoustic mode of flow behind FA" (near F), and the same should apply for the flow mode when the point of intersection between the polars lies below W. The boundary state for flows with a centered negative-pressure wave is represented by the state where the polar for FA' passes through W (Fig. 1d). If the point of intersection lies above W, there can be direct conjugation in accordance with Eq. (1.4) (Fig. 1e).

The criterion for the transition from the first mode to the second is that the polar curves intersect at W, where

$$\theta_p = \theta_F, \quad n\varepsilon_p = n_Q\varepsilon_F, \quad (N_F - q_F)^2 + N_F^2 \operatorname{tg}\beta_F = c_F^2.$$

Here N_F is the propagation speed for FA" and q_F is the velocity difference for the particles at it, with c_F the speed of sound behind FA" and β_F the angle between FA" and the normal to the d_1d_2 plane (all quantities near F).

We now consider the flow near the $d'd_1'$ contact line. Calculations [6, 9] show that the transient response is followed by a vortex arising near the contact line because the SW interacts with the end region of layer Q, where vorticity is generated because the isochores and isobars are not collinear as the SW passes along the layer. The circulation in that vortex can be estimated from Bjorknes' theorem. Figure 1 shows the integration contour ($dd_1d_1"d"$), with dimensions governed by the size of the circular vortex with diameter of the order of h forming within the layer. The SE travels that distance in a time $t_c \approx h \cos\alpha/N_1$. For glancing incidence

$$\Gamma = -\int_0^{t_c}\oint \frac{dp}{\rho}\,dt \approx -\frac{\Delta p_r \Delta\rho}{\rho_0\rho_Q}\,t_c$$

$$(\Delta p_r = kp_r - p_0,\ \Delta\rho = \rho_0 - \rho_Q,\ k \approx \rho_0/\rho_r \approx \rho_Q/\rho_Q^0).$$

Vorticity is also produced in the further SW motion (the intensity has the same order Γ on any segment d_1d_2 having length h), which is concentrated in a vortex pattern along the d_1d_2 contact plane. For $\alpha \neq 0$, the vortex circulation falls sharply as α increases because t_c falls. For $\alpha = 45°$, all the forward part of the layer with length h is covered by the shock front instantly. The incident wave AK interacts with the negative-pressure wave DD_1K', with A being the triple point. A second triple point is provided by A'. This λ-configuration arises because the precursor (A'F shock front) interacts with the AA' shock front.

We now turn to the precursor in Q. The centered negative-pressure wave is a local supersonic zone in a subsonic flow behind the FA" front in the coordinate system linked to A", so no matter what the conjugation details in the F'FA"d' region, one has a nearly constant flow, or rather, an expanding one (expansion angle θ_p), which implies a slowing flow, in which the pressure should rise in the A"d' region.

2. The motion is determined by p_0, ρ_0, h, ρ_Q, n, n_Q, p_1, from which one can formulate four independent dimensionless combinations: ε_1, c_Q/c_0, n/n_Q, n. Here h does not appear, which shows that the flow structure (in x/h, y/h, c_0t/h coordinates) is independent of h. Parameter n/n_Q for minor differences of about 15% between n and n_Q has little effect on the flow type. The main quantities governing the flow remain ε_1, c_Q/c_0, n.

An apparatus has been built (Fig. 2) to examine the motion, which provides SW with preset intensity uniformly distributed over the planar surface with which the wave interacts, with the gas layer having constant density. It is fitted with a shock tube, a high-voltage discharge system, and a set of measuring equipment. The single-stage diaphragmed shock tube is an 85 × 125 mm rectangular channel and gives an SW with relative intensity in the range $0.07 < \varepsilon_1 < 3$.

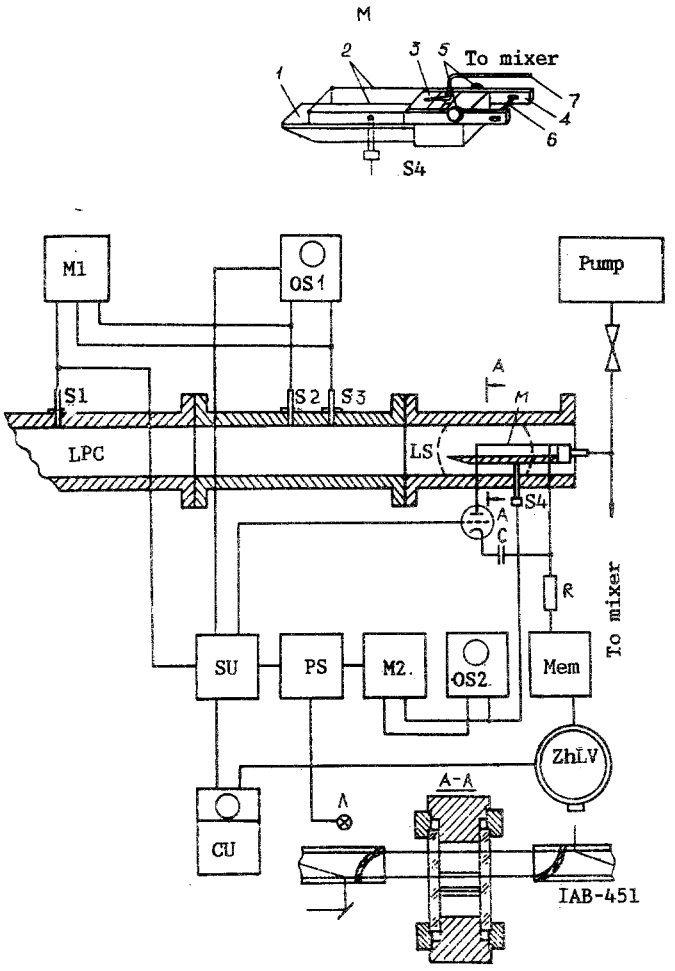

Fig. 2

The equipment enables one to photograph the interaction with the rigid surfaces and to measure the pressure differences behind the incident shock fronts. The system for measuring those differences consists of the sensors S1-S4, timers T, and the oscilloscopes OS1 and OS2. The schlieren method and high-speed photography are used to record the flow behind the fronts (the IAB-451 in a unit with the ZhLV equipment or camera). Flash lamps were used. The measurement section 0.34 m long was equipped with illuminators and with holes for inserting the pressure sensors and a mechanism for mounting the model M. The main part of M is a flat plate 85 × 200 mm with a sharpened leading edge. In glancing experiments ($\alpha = 0$), that edge encounters the SW. With $\alpha \neq 0$, the edge rests on the lower wall of the tube.

The plate is coated with a gas lighter than air, namely a nitrogen–helium or nitrogen–hydrogen mixture, whose composition may be varied to give a density and a speed of sound equivalent to those for air at 350-2700°C [8].

There are some additional units (Fig. 2) to produce a layer with given geometry: 1 – a rigid wedge, with the upper plane the reflecting one; 2 – a wire frame; 3 – a step rigidly coupled to the plate, which is a continuation of it; and 4 – knife-edge plates hinged to the step. The frame of the wire framework is welded to the plates. The parts of the framework perpendicular to the outer frame are made of flexible wire and do not interfere with the movement, which is provided by screws 5 and spring 6. The movement part provided by the latter is needed to press the wire frame onto the illuminators in the measurement section. There is a channel through the step linked by the flexible hose 7 to the mixer for the gas mixture. The plate bears the pressure sensor S4. The sensing surface coincides with the reflecting surface.

Layer Q is produced by blowing a prepared nitrogen–helium or nitrogen–hydrogen mixture under a soap film. The mixture is supplied through the hose from the mixer to a soap bubble

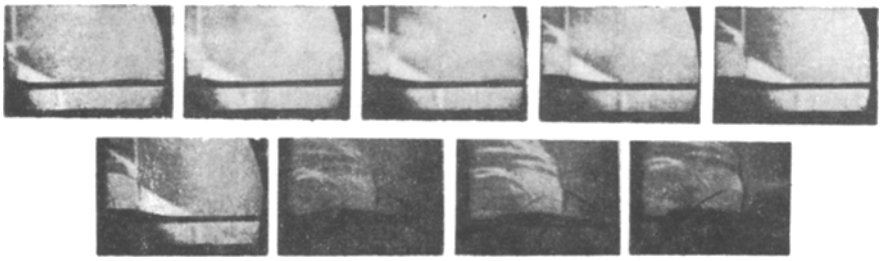

Fig. 3

resting on the reflecting plate. To make the bubble, the upper surface of the plate and a wire in the framework are treated with a special soap solution [11]. The film is tensioned from the hole in the step linked to the hose. After this preliminary procedure, the cavity is flushed and filled with a mixture of given density. The mixture supply is stopped when the film in the bubble encompasses the framework. The pump balances the pressure in the cavity to the outside pressure, so the film is flat on each face of the parallelepiped bounding the cavity containing the light gas.

Note. The liquid film is disrupted in the front motion or before it arrives (in the first series of experiments, the film was broken about 1 msec before the interaction started by local heating from contact with a wire heated by a current pulse), which is a difference from [4], where an organic film was used, and which thus enabled us to examine the motion almost without external distorting factors.

After the diaphragm ruptures, the SW propagates along the channel and produces a series of signals at S1-S4. The photography is accompanied by displaying the flow pattern with the IAB-451 (Töpler patterns), while the sensor measures the pressure at the reflecting plate. The additional information not only enables one to determine the pressure amplitude behind the precursor wave in Q but also to define the speed of the precursor accurately. The oscilloscope OS2 enables one to determine the time of motion from the flash to the arrival of the shock front at the sensor, as it is triggered at the same time as the spark source, or the same can be done more accurately with the M2 meter. Independent measurements are provided for the pressure amplitude and the SW speed in layer Q in order to establish the initial speed of sound c_Q in Q and thus to compare the actual value with that supplied in the gas layer. The density and speed of sound in the mixture may be determined by calculation and by direct measurement. The first is derived from the mixture composition.

3. Glancing Incidence. Figure 3 shows the SW propagation along a surface coated with nitrogen–helium mixture, layer thickness 15 mm, length 180 mm, $c_Q/c_0 = 1.99$, $\varepsilon_1 = 0.710$, recording speed 288,600 frames/sec.

Such recordings gave the speed of the precursor in Q (speed of point A"), as well as the speeds and displacement directions for the triple points A and A'. The precursor speed was determined from a plot in $(x_{A"} - x_r, X_A - x_r)$ coordinates, in which $x_{A"}$, x_A are the coordinates of the precursor in Q and the incident SW, with x_r = const the coordinate for the fixed reference point. Similar techniques gave the speeds and paths for the triple points. With computer processing, the accuracy is 2-3% in determining the speed of a given point as a function of time.

The cinematography showed that an initial part about (1-1.5)h long, in which the shock-wave pattern is established, is followed by the paths of the triple points becoming rectilinear, i.e., the motion is of quasi-self-similar character, which was first noted in [4] and then in [7-9], and which enables one to simplify the method and improve the accuracy by transferring from single-frame recording to recording on 35 mm film.

The Töpler patterns and the pressure waveforms give not only the kinetic parameters but also the speed of the precursor in the layer $N_{A"}$ and c_Q, the initial speed of sound in layer Q, which is independent of the composition measurements, as well as the profile in the pressure p_Q (or ε_Q) behind the front at the surface S and the speed $q_{A"}$ of the particles behind the precursor front. The front motion time can be derived from the oscillogram

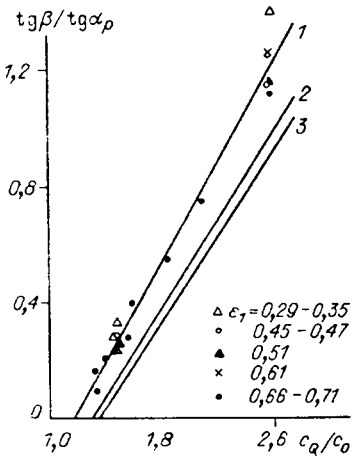

Fig. 4

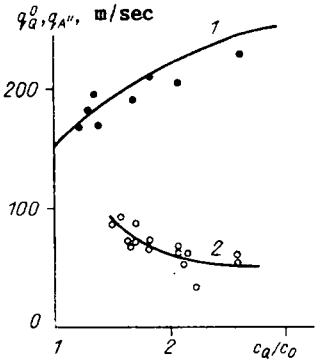

Fig. 5

or from the M2 meter (Fig. 2); the distance needed to determine N_A'' is derived from the Töpler pattern. The values of c_Q, q_A'' are derived [10] from

$$c_Q = N_{A''}\Big/\sqrt{1+\frac{n_Q+1}{2}\varepsilon_{A''}},\quad q_{A''} = c_Q\varepsilon_{A''}\Big/\sqrt{1+\frac{n_Q+1}{2}\varepsilon_{A''}}, \tag{3.1}$$

in which the pressure step at the precursor front $\varepsilon_A'' = (p_A'' - p_0)/n_Q p_0$ is measured by S4. Figures 4 and 5 show some results. Figure 4 shows the path measurements: the inclination angle of the precursor in air α_p and the inclination angle β of triple point A' (Fig. 1) as functions of mixture composition; the curves have been derived from

$$\mathrm{tg}\beta/\mathrm{tg}\alpha_p = c_Q/N_1 - 1 \tag{3.2}$$

(1-3 for ε_1 = 0.32; 0.61; 0.69). Formula (3.2) has been derived for the case where the precursor is a weak SW ($N_A'' \sim c_Q$) subject to self-similarity in the motion and the obvious relation $(N_A'' - N_1)\tan\alpha_p = N_1 \tan\beta$.

Figure 5 shows results from the cinematography (Töpler patterns) for the speed of the center O of the vortex formation for ε_1 = 0.66-0.72 and various c_Q/c_0 (filled points); line 1 is $q_Q^0 = q_Q^0(c_Q/c_0)$ for ε_1 = 0.71 as calculated from Eq. (1.3).

Measurements made for $0.3 < \varepsilon_1 < 1.19$ and $1.22 < c_Q/c_0 < 2.74$ showed that the instantaneous pattern for the SW fronts coincide qualitatively with that derived numerically in [4, 6, 9].

For all ε_1 and c_Q/c_0 in those ranges, the interaction gave rise to the precursor FA" in Fig. 1; outside the layer, this corresponded to the precursor A'F. The measurements show that the relative pressure difference ε_A'' at the SW front in layer Q near S was much less than in the incident wave; ε_Q increases continuously away from FA". The pressure profile means that the particle velocity behind the front should increase, which is confirmed by direct measurements on the speed of the vortex formation (Fig. 5), whose center had a speed (Fig. 3) close to the speed of the contact discontinuity f'd$_1$'d and thus, to the speed $q_Q^0 = q_r$ of the adjoining particles. Figure 5 also shows the velocities of the particles q_A'' at the precursor front at A" for $\varepsilon_1 \approx 0.7$ (open points, curve 2) as calculated from Eq. (3.1). It is evident from Fig. 5 that the particle speed in the layer as reckoned from FA" towards F'd$_1$'d (Fig. 1) varies from q_A'' to q_Q^0. The general motion pattern is self-similar or nearly so. The experimental basis for this is not merely the rectilinearity in the motion of A and A' [4, 6, 8, 9] but also the linearity of $x_A'' = x_A''(x_A)$, which shows that there was no damping for FA" and the precursor A'F.

The self-similar state is set up at (1-1.5)h from the vertical boundary of Q (dd$_1$ in Fig. 1). At that time, one gets all the characteristic wave features, with the precursor in Q, the precursor in the external medium, the triple points A and A', and the vortex formation closing the layer, that is, the general structure in those flows. There are some particular features in glancing incidence. The SW begins to interact with the layer with the decomposition of the discontinuity, during which a negative-pressure wave arises behind the front of the incident wave together with an SW in the layer. The pressure amplitude and the speed of the contact discontinuity (particle speed q_r) are governed by ε_1, c_Q/c_0,

Fig. 6

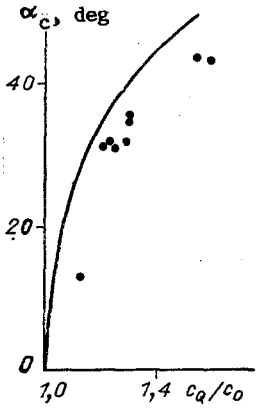

Fig. 7

n/n_Q, and n, and the measurements showed that the speed of the contact discontinuity remains unchanged at q_r, the speed that arises when the incident discontinuity splits up. This is as though a liquid piston moving with a constant velocity acted on the light gas throughout the motion. As ε_1 and c_Q/c_0 increase, the speed q_r of that piston may attain N_1, and the light gas then does not penetrate behind the incident SW front. The condition for realizing that state $N_1 = q_r$ for a layer of helium (equivalent to air at 2229°C) is met for $\varepsilon_1 \approx 5$, while for a layer of hydrogen (equivalent to air at 3909°C) for $\varepsilon_1 \approx 2.85$ [8].

4. The measurements with $\alpha \neq 0$ were made with $1.23 \leq c_Q/c_0 \leq 2.5$; $13° < \alpha < 43°$; $0.3 < \varepsilon_1 < 1$.

Figure 6 shows Töpler patterns indicating three instantaneous (exposure time ~0.5 μsec) substantially different patterns occurring behind the incident waves at various α (Fig. 1). Figure 6a shows no precursor, since $N_1/\cos\alpha > N_F$ along the surface, whereas it occurs for $N_1/\cos\alpha < N_F$. The latter state corresponds to Fig. 6b. The maximum angles of incidence $\alpha_c = \alpha_c(c_Q/c_0, \varepsilon_1)$, for which the precursor occurred are called critical angles for the light-gas layer, which correspond to $N_1/\cos\alpha \approx N_F$. The Töpler pattern corresponding to the critical angle is shown in Fig. 6c. Figure 7 shows the measured critical angles for $\varepsilon_1 \approx 0.7$. The solid line shows $\alpha_c = \alpha_c(c_Q/c_0)$ derived from the approximation $\alpha_c = \arccos c_Q/c_0$) (itself derived on the assumption $\varepsilon_1 \approx \varepsilon_F$).

For $\alpha > \alpha_c$, when there is no precursor, the perturbations from the surface do not attain the points where the incident SW intersects the boundary, and the wave pattern corresponds to regular refraction of the SW at the boundary between two gases in the absence of a surface [12-16].

LITERATURE CITED

1. K. E. Gubkin, "Shock-wave propagation," in: Mechanics in the USSR over 50 Years [in Russian], Vol. 2, Nauka, Moscow (1970).
2. E. G. Popov and M. A. Tsikulin, Emissivity of Strong Shock Waves in Gases [in Russian], Nauka, Moscow (1977).
3. E. J. Gion, "Plane shock, interacting with a thermal layer," Phys. Fluids, 20, No. 4 (1977).
4. S. M. Bakhrakh, B. A. Klopov, et al., "Collapse of a gap in a wall on normal incidence of a shock wave," ChMMSS, 9, No. 5 (1978).

5. L. G. Gvozdeva and A. I. Kharitonov, "An interferometric study on shock-wave motion along a heated surface in a shock tube," in: Optical Methods of Examining Gas Flows and Plasmas [in Russian], ITMO AN BSSR, Minsk (1982).
6. B. N. Gordeichik and I. V. Nemchinov, "Precursor formation in shock-wave interaction with a thermal layer," in: Applied Mechanics Methods [in Russian], Dep. VINITI No. 2529-84, April 20, 1984, Moscow (1983).
7. V. I. Artem'ev, I. E. Markovich, et al., "Two-dimensional self-similar motion of a strong shock wave above a heated surface," Dokl. Akad. Nauk SSSR, 293, No. 5 (1987).
8. B. I. Zaslavskii, S. Yu. Morozkin, V. R. Shlegel', and M. D. Shcherbin, The Motion of a Planar Shock Wave Along a Rigid Surface Coated with a Light-Gas Layer [in Russian], Dep. VINITI No. 3965-V87, June 4, 1987, Moscow (1987).
9. V. I. Bergel'son, I. V. Nemchinov, et al., "Self-similar precursor development ahead of a shock wave interacting with a thermal layer," Dokl. Akad. Nauk SSSR, 296, No. 3 (1987).
10. R. Courant and C. Friedricks, Supersonic Flow and Shock Waves [Russian translation], Izd. Inostr. Lit., Moscow (1950).
11. C. V. Boys, Soap Bubbles [Russian translation], Gostekhizdat, Moscow (1934).
12. L. F. Henderson, "The refraction of a plane shock wave at a gas interface," J. Fluid Mech., 26, No. 3 (1966).
13. L. F. Henderson and A. K. Macpherson, "On the irregular refraction of a plane shock wave at a Mach number interface," J. Fluid Mech., 32, No. 1 (1968).
14. L. F. Henderson, "On shock impedance," J. Fluid Mech., 40, No. 4 (1970).
15. A. M. Abd-el-Fattah, L. F. Henderson, and A. Lozzi, "Precursor shock waves at a slow–fast gas interface," J. Fluid Mech., 76, No. 1 (1976).
16. A. M. Abd-el-Fattah and L. F. Henderson, "Shock waves at a slow–fast gas interface," J. Fluid Mech., 89, No. 1 (1978).

HYDRODYNAMIC ANALYSIS OF THE PROCESS OF MAKING THREE-LAYER OPTICAL FIBERS AND CALCULATION OF THE FIELD OF ELASTIC STRESSES AND BIREFRINGENCE

A. L. Yarin

UDC 539.377+532.63+681.7.068.2

One of the methods used to make semifinished products for the manufacture of polarization-maintaining optical fibers is based on the use of the surface tension of glass in the liquid state [1]. The initial cross section of the semifinished product is shown in Fig. 1, where the region 0 corresponds to the core through which the signal propagates. The numbers 1 and 2 denote the straining and cladding sheaths, which are designed to create a stress state in the core. Part of the clad is removed – as shown by the dashed lines in Fig. 1, for example – and the semifinished product is placed in a furnace and heated. During heating, the straining and cladding sheaths become liquid and the surface tension at the boundary Γ_2 begins to round it off. The resulting flow of molten glass deforms the boundary Γ_1, which is subjected to a low surface tension. The deformation of this boundary causes it to lose its circular form. Meanwhile, the core remains solid and boundary Γ_0 remains unchanged. After completion of the process of rounding-off of the boundary Γ_2, a semifinished product with a noncircular boundary Γ_1 is obtained. Due to the difference in the thermoelastic properties of the materials in the straining and cladding layers of the semifinished product (and optical fiber), an anisotropic field of elastic stresses is created along with the associated birefringence. Accordingly, the core becomes capable of transmitting signals with a certain polarization.

Moscow. Translated from Zhurnal Prikladnoi Mekhaniki i Tekhnicheskoi Fiziki, No. 3, pp. 23-30, May-June, 1990. Original article submitted June 6, 1988.

0021-8944/90/3103-0361$12.50